Risdonne *et al. Herit Sci* (2021) 9:70
https://doi.org/10.1186/s40494-021-00533-0

Heritage Science

RESEARCH ARTICLE Open Access

A multi-analytical study of historical coated plaster surfaces: the examination of a nineteenth-century V&A cast of a tombstone

Valentina Risdonne[1,2], Charlotte Hubbard[3], Johanna Puisto[2] and Charis Theodorakopoulos[1*]

Abstract

A multi-analytical study was designed to characterise historical coated plaster surfaces. The method was applied to investigate the surface coatings of the nineteenth-century plaster cast of the tombstone of the Presbyter Bruno that belongs to the Victoria and Albert Museum collection. At first, selected samples of the object were examined with Visible Light Reflectance and Ultra-Violet Fluorescence Optical Microscopy (VLR- and UV*f*-OM respectively) and Scanning Electron Microscopy (SEM) demonstrating a consistent stratigraphy featuring a bulk, an interface and an uppermost layer. The latter layer appeared to consist of an aged coating and dirt. Overpainted and repaired areas of the object generated samples that had additional layers on top of the aforementioned stratigraphy. A layer that seemed to be an additional surface varnish or a coating that had not been absorbed to the bulk has been observed in a couple of samples. Elemental characterization was carried out with energy dispersive X-ray spectroscopy (EDS) and further analyses were performed with X-ray diffraction (XRD) and Fourier-transform infrared (FT-IR) spectroscopy with focal plane array (FPA) imaging which confirmed that the bulk of the object is made of gypsum plaster containing mostly silicate and carbonate inclusions. Gas chromatography/mass spectrometry (GC/MS) and pyrolysis-GC/MS with extraction methods based on n-propanol followed by pentafluoropropionic anhydride (PFPA), tetramethylammonium hydroxide (TMAH) and 3-trifluoromethylphenyltrimethylammonium hydroxide (m-TFPTAH) were performed to detect organic media. The results suggest that the organic medium used for the surface coating is a diterpenic resin that contained silicon, aluminium and traces of other inorganic elements. The organic medium of overpainted areas was based on alkyd resins and the in-paints were characterised as a blend of silicon and barium at varied concentrations. This multi-analytical approach can generate a better understanding of manufacturing, component materials and conservation issues of coated plaster objects.

Keywords: Coated plaster casts, Organic coatings, Multi-analytical examination, Optical microscopy, Scanning electron microscopy (SEM), Fourier-transform infrared spectroscopy (FT-IR), X-ray diffraction (XRD), Energy dispersive X-ray spectroscopy (EDS), Pyrolysis-gas chromatography/mass spectrometry (py-GC/MS)

Introduction

This work represents a pilot case study designed to establish a wider campaign of sampling and scientific analyses of the surface layers of the casts produced in the nineteenth century, in the framework of a collaborative doctoral partnership of Northumbria University with the V&A Museum (AH/R00322X/1) [1]. Part of the project

*Correspondence: charis.theodorakopoulos@northumbria.ac.uk
[1] Department of Arts, Science in Conservation of Fine Art, Northumbria University, Burt Hall, Newcastle City Campus, NE1 8ST Newcastle upon Tyne, UK
Full list of author information is available at the end of the article

Fig. 1 Plaster cast of the tombstone of Presbyter Bruno (V&A Accession Number: REPRO.1873-380), ca. 1873. © Victoria and Albert Museum, London/as specified by the rights holder

focused on the characterisation and the ageing characteristics of the original coatings of historical plaster casts [2]. In the nineteenth century, the plaster cast replicas of famous artworks were used extensively in schools and museums [3–5]. The aim was to educate and inspire those who studied or appreciated art. They were also fashionable among the more affluent people who decorated their homes with plaster ornaments and copies of well-known sculptures [6–9].

The object of this study is a nineteenth-century plaster cast of the Tombstone of Presbyter Bruno, part of the Victoria and Albert Museum (V&A) collection (Museum Accession Number REPRO.1873-380,[1] Fig. 1) and displayed in the Cast Courts (Gallery 46A). The 'Copy of the Tombstone of Presbyter Bruno' is a plaster replica of an original tombstone from the Cathedral of Hildesheim (Germany), by Friedrich Heinrich Nicolaus Küsthardt the elder (Göttingen 1830–Hildesheim 1900) [10, 11].

The original tombstone is dated 1194 and is still located in Hildesheim Cathedral. In 1873, the Museum acquired several plaster casts of key sculptural decorations in Hildesheim Cathedral, all produced by Küsthardt, among them, the tombstone, purchased directly from Küsthardt in 1873 for £6.

Küsthardt's plaster copy of the tomb slab, 218.5 cm high by 77.0 cm wide, is currently displayed between a mix of casts of different origin, as well as a variety of early Christian monuments and other reproductions from Hildesheim Cathedral. The cast is mounted on a wooden display frame, and on its reverse, is another German reproduction depicting an upper left portion of a wooden doorway from the Church of St Maria im Kapitol, in Cologne (the original was carved c. 1065 by an unknown carver) [12].

Neither cast appears in any of the early photographs of the V&A galleries. Yet later pictures of Küsthardt's cast on its own, held in the V&A curatorial department, reveal that it was formerly mounted upright on a different backing, with metal brackets supporting its base (Fig. 2). The brackets were later removed which explains the current losses to the plaster under the relief. The photographs also reveal a series of exposed metal screws at the front to attach the plaster to its wooden or metal supporting frame (Fig. 2). Many of the casts in the collection have been fixed to their supports with similar metal screws. Often the screw-heads have been filled and retouched to conceal them, which is the case with Küsthardt's piece. The positions of fixings are easy to recognise, as the filler is often slightly proud and, in many instances, split around the edges. This is due to the corroding metal or shrinkage of the filler. Also, the overpaint is often of a slightly different colour, either because of ageing, or the retouching was aimed to be noticed, in case the objects needed deinstalling.

A close examination shows that the cast is made of three sections, which sit directly on top of one another, with pieces of wood wedged between them. Interestingly, the original sandstone slab, which is mounted on the south wall of the choir at Hildesheim cathedral, is carved from a single block of stone, although it has additional stone sections added at the top and on its base, which have not been replicated in the V&A copy. Also, by comparing archival images of the original slab, some of the losses to the original stone surface do not show on the cast, as can be observed. It may be that some of the surface details on the original stone were lost after the cast was made, or some of the details on the cast were later reworked.

[1] The Museum nos. can be used to find the objects in the V&A Website—Search the Collections (2020).

Fig. 2 An early photograph of the cast shows that metal brackets were used to hold it upright (orange arrows). In this early image the screws that secure it in position are still visible (yellow arrows)

The top section of the cast has various vertical and horizontal lines under the arch surrounding the Christ's head. The lines have been sanded down, suggesting the cast could have been made using a piece mould technique. Piece moulds tend to leave raised seamlines on casts and, they were often disguised by sanding them down [2].

The outer edges of the cast have been covered with painted plywood sheeting, to conceal their unevenness (Fig. 3). Interestingly, the edges of the original stone slab are finely finished. Many casts in the V&A collection were not meant to be viewed all around. They are often unfinished at their sides and the top and were later covered with either fabric, card, wood, or metal to disguise the exposed areas and to protect them from dust.

A close examination of the underside reveals that there is a small section of metal visible at the back of the cast, on the left side. It could be what remains of the old bracket after it was cut back, or it could be part of a larger metal support. Metal and wooden supports are commonly found on the backs of the plaster casts. Using a metal detector, it was revealed that the top and middle parts of the cast have less metal backing support than the lower part of the cast.

Küsthardt's cast has been restored on several occasions since it came to the museum some 148 years ago. Unfortunately, there are no records of any of the previous restorations, but a close examination reveals that numerous localised areas on the surface have been repaired with a filler and touched up using different paints and colours at different times. It was fairly common before the 1970s, for the restorers, not to document their treatments. However, many casts in the collection have names and dates pencilled on discreet areas on the object's surface. This information helps to pin down when objects were restored and by whom. Casts also might have traces of old materials on their surfaces: residue of soap or residue of casting materials such as gelatine, or items at their backs including, packages of soap, pigments, cloths, sponges, tools, newspapers, letters, food packaging etc. Unfortunately, due to the framing of the cast, it is difficult to observe the back of Küsthardt's cast.

Although there are no signatures or dates on Küsthardt's cast visible at the front, apart from museum numbers near the base and at the top, and Küsthardt's company label can be found on the top right corner on the lower section. It reads: 'Bildhauer, FR Küsthardt, Hildesheim' in embossed lettering (Fig. 3).

There are also many tool-marks and possibly fingerprints where the plaster surface has been worked on. Several raised areas, particularly on the lower sections, are also covered in pencil marks. These were probably left by various artists and students who sketched and drew the object in the galleries ever since they were built. Similar pencil marks on the plaster surfaces have been observed by the authors in art schools' collections, as for example the one in the Hatton Gallery in Newcastle upon Tyne.

Research on plaster cast objects often remains unpublished at large within the records of collection holding organisations and individual case studies fail to represent the breadth and complexity of the materials that can be found in the eclectic cast collections due to case

Fig. 3 The cast still retains the stamp of the workshop of Friedrich Küsthardt (**a**). A closer look at the object revealed the plywood sheeting used to conceal the cast's edges unevenness (**b**). An accidental spillage was highlighted under UV illumination from the area where sample 12 was taken (**c**)

specificity [13–16], whereas often useful insight on the properties of materials can be found in studies on building decorative materials [17], such as plasterworks [18] and mortars [19]. Megens et al. [20], on the other hand, have demonstrated that systematic elemental analysis is required to uncover the provenance and composition of plaster used to replicate art and decorative objects: traces analysis, size and distribution of porosity and mineral shape and growth can be characteristic of a particular group of artefacts. Gypsum plaster (calcium sulfate, $CaSO_4{\cdot}0.5H_2O$) has consistently been found as the main component of the bulk of the nineteenth-century plaster casts [2]. However, organic (such as resins and gums) and inorganic compounds (such as clay, sand, lime), as well as larger structural elements (such as fabrics, wooden or metal batons or even bones) were combined and added during the plaster production, as used to improve mechanical properties, such as hardness and water resistance or to control setting time and the casting procedure [2, 20]. The complexity of the organic and inorganic blended compositions in the plaster artefacts suggests that a multi-analytical approach would be more appropriate. For example, Field emission gun–scanning electron microscopy (FEG–SEM), XRD and Particle induced X-ray emission (PIXE) allowed the examination of Renaissance stucco related materials, which indicated that the composition of the mineral phases influences its sustainability and sensitivity to moisture sorption processes [21].

The full characterization of the materials of the cast will also provide fundamental information for the deterioration processes and guide conservation decisions. Typical damage observed is related to environmental conditions or unsuitable protection and handling. Plaster objects may become heavily soiled and covered with dirt and dust layers. Exposure to high relative humidity levels

causes the migration of deposits into the plaster's porous structure. Due to alternating swelling/shrinking cycles in time and the fragility of plaster materials, objects often lose their texture, crack or break into fragments [22].

This study aims to characterise the materials used to produce the surface layers of the plaster casts, either to provide the plaster with certain properties and to achieve the desired appearance. While VLR- and UV*f*-OM allowed the identification of the stratigraphy, SEM–EDS and XRD were used to monitor the inorganic composition and FT-IR and (py)–GC/MS to characterise the organic components. Trace analysis to investigate the provenance of the object were not carried in this study, being beyond the scope. The study of the object served as a pilot study for the determination of an analytical strategy for the examination of the surfaces of plaster casts that will eventually allow a better understanding of the workshops' practices in place in the nineteenth century and define more specifically targeted conservation methods. Archival information was available in the Registry of Reproductions of the V&A Museum (1873), in the museum Collection Management System (CMS) and the V&A archive currently at Blythe House, London.

Experimental

Sampling

A total of thirteen samples from selected areas were taken, according to British Standard BS EN 16085:2012 (ISBN 978 0 580 70588 5). Before the sampling, a careful survey was performed to prevent any risk and to minimize the quantity of sample collected, which was never larger than 1.0 mm across, and maintain the integrity of the object. The sampling procedure was fully documented [23]. The sampling areas were determined by many factors, such as accessibility and significance, but also avoiding foreground areas. The samples were taken from areas of pre-existing loss and undercuts or marginal areas. The utmost attention was given to ensure that the samples were collected limiting any contamination. Before being stored in the vials, the samples were numbered with the museum accession number and the progressive sampling number, which is used throughout the study to identify the samples, as follows: *MUSEUM ACCESSION OBJECT NUMBER_PROGRESSIVE SAMPLE NUMBER*.

Technical photography

Regular visible photographs were taken with a Panasonic DCM-FZ38 camera under the gallery's normal illumination (i.e., diffuse lighting, skylight window natural light and mixed artificial illumination). Colour and dimension references were ensured through the Past Horizons® Credit Card Photography Scale. The images were processed with Adobe Photoshop® CC 19 and white-balanced through the Past Horizons® Credit Card Photography Scale. The objects were also rendered in Autodesk® AutoCAD® 2019 for mapping purposes (Fig. 4).

Stereomicroscopy

A StereoZoom® LEICA S6D stereomicroscope was used to observe the samples, to understand the shape of the samples, the position of the layer in the stratigraphy and to define the processing of the sample. The Leica S6D Stereomicroscope has a 10× eyepiece and the objective magnification range from 0.63× to 4.00×. When possible, samples were split into two parts: one fragment was embedded in polyester resin to allow the observation of the stratigraphy and the analysis of the layers and the other was put aside for destructive analyses.

Samples for cross-sectional analysis

The samples were embedded in Alec Tiranti™ Ltd clear casting resin, which required 48 h to cure and harden. Alec Tiranti™ Ltd clear casting resin consists of styrene and methyl methacrylate/polyester resin (Product Code: 405-210) and liquid hardener (BUTANOX M-50 methyl ethyl ketone peroxide, solution in dimethyl phthalate—Product Code: 405-810) in the proportion 4 mL: 1 drop.

Visible light reflectance (VLR) and ultraviolet fluorescence (UVF) optical microscopy (OM)

Optical microscopy was performed with an Olympus BX51 Metallurgical Microscope equipped with four objectives (magnification of ×5, ×20, ×50 and ×100), and an ×10 eyepiece. 50 µL of white spirit were added on the surface of the cross-section to improve the saturation under the microscope. The microscope is equipped with a 6-cube filter turret which allows operating the system in reflected visible light (brightfield and darkfield mode) and reflected UV light (365 nm) using a 100 W mercury burner.

X-ray diffraction (XRD)

The XRD analyses were performed with a Rigaku SmartLab SE equipped with a HyPix-400, a semiconductor hybrid pixel array detector and a Cu source. The analyses were performed in Brag-Brentano geometry mode, with 40 kV tube voltage and 50 mA tube current. The diffractograms were processed with SmartLab II software. The data was compared to the data available in the RUFF™ database [24] and the Crystallography Open Database (COD) Database [25].

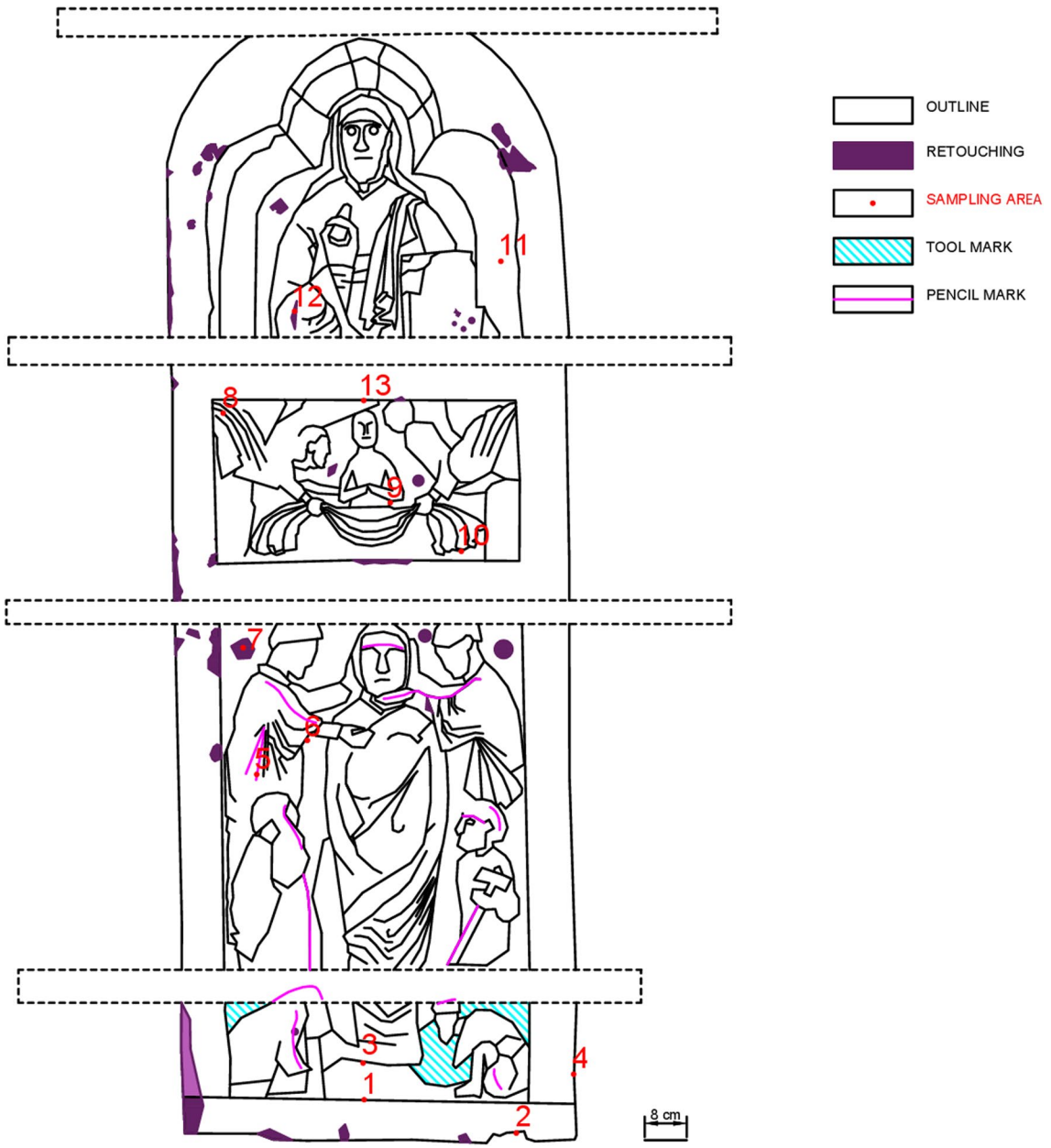

Fig. 4 The outline of the Tombstone drawn in AutoCAD with marked sampling sites (red), pencil marks (pink) and the areas showing retouching (purple) and tool marks (blue)

Scanning electron microscope (SEM)—energy dispersive X-ray spectroscopy (EDS)

The SEM–EDS analyses were performed with a field emission TESCAN MIRA 3 with gigantic chamber. The SEM is equipped with a back-scatter detector (BSE) and back-scatter in-beam detector (In-beam BSE). For the EDS analytical part, it has an Oxford Instruments setup: Software: AztecEnergy, X-ray detector X-Max 150 mm^2 and X-ray detector X-Max Extreme, low energy detector for thin films, high resolution and low voltage. The samples were analysed by SEM–EDS Low Vacuum Mode (10–15 Pa). EDS Mapping and data processing were performed with Aztec Oxford software. A fragment of sample 2 was mounted on appropriate support, adhered with silver paint and coated with a layer of platinum (5 nm thick). This sample preparation is required when high vacuum SEM–EDS (1.5×10–2 Pa)

is performed. This mode allows a higher magnification with a better definition.

Fourier-transform infrared spectroscopy (FT-IR) with focal plane array (FPA) imaging

A Perkin Elmer Frontier FT-IR spectrometer (350 cm^{-1} at a best resolution of 0.4 cm^{-1}) was used, equipped with a UATR Diamond/ZnSe ATR accessory and combined with a Spectrum Spotlight 400 FT-IR microscope equipped with a 16 × 1 pixel linear mercury cadmium telluride (MCT) array detector standard with InGaAs array option for optimised NIR imaging. Spectral images from sample areas are possible at pixel resolutions of 6.25, 25, or 50 µm. The Perkin Elmer ATR imaging accessory consists of a germanium crystal for ATR imaging. These run with Perkin Elmer Spectrum 10™ software and with SpectrumIMAGE™ software. Baseline and Kubelka–Munk corrections were applied to the raw data acquired in diffuse reflectance (DR). The FT-IR spectrometer range is 350–4000 cm^{-1} in the ATR mode and 650–4000 cm^{-1} in the DR mode.

Gas chromatography/Mass spectrometry (GC/MS) and pyrolysis-GAS chromatography/mass spectrometry (py-GC/MS)

The instrument used for GC/MS is a Thermo Focus Gas Chromatographer with DSQ II single quadrupole mass spec. The column is an Agilent DB5-MS UI column (ID: 0.25 mm, length: 30 m, df: 0.25 µm, Agilent, Santa Clara, CA, USA), fitted with a Pyrola 2000 Platinum filament pyrolyser (PyroLab, Sweden). The helium carrier gas flow rate was 1.5 mL/min with a split flow of 41 mL/min and a split ratio of 27. The temperature of the detector was set at 280 °C and the inlet injector temperature to the GC was kept at 250 °C. The pyrolysis chamber was heated to 175 °C, and pyrolysis was carried out at 600 °C for 2 s. Samples derivatization was necessary for GC/MS [26–30] and carried with *n*-propanol followed by pentafluoropropionic anhydride (PFPA) [31], to derivatise protein component of proteinaceous paints and adhesives, while yielding the propyl esters of fatty acids derived from lipids and diterpenoid acids derived from natural resins and thus allows the choice of a single method for the analysis of artists media which contain either oils or proteins or mixtures of both proteins and oils or even resins. 1 mg of pulverised sample was hydrolysed in 150 µL of Hydrochloric acid (HCl) and the excess Oxygen was removed. The solution was heated at 90 °C for 3 days and placed in a vacuum desiccator for 24 h to remove the acid. After 180 µL of propan-1-ol: acetyl chloride (3:1) were added, the solution was heated at 110 °C for 45 min, then at 50 °C for 30 min. The reagent excess was then removed via nitrogen. The residue was dissolved in 50 µL 0.2% pyridine and 150 µL of dichloromethane (DCM) and 150 µL perfluoropropionic anhydride (PFPA) were added before heating at 110 °C for 15 min [31]. The sample was then injected into the column with the aid of a micro-syringe and the MS thermal Programme (3) was set as follows: Seg1 start 13.00 Scan events MS, Heated zones Ion Source 250 °C, Detector Gain 1.21·105 (Multiplier Voltage 1025 V). Oven: Initial temp 60 °C hold 2 min Ramp 1 6.0 °C/min (rate), 250 °C, hold 0 min. Ramp 2 25 °C/min, 300 °C, 20 min hold. Mode: split. A pulverised sample of the order of 0.5 mg was either directly derivatised in an aliquot of 1 µL of 25 wt% in methanol tetramethylammonium hydroxide (TMAH) and placed on the Pt filament, or methylated with 3-trifluoromethylphenyltrimethylammonium hydroxide (5 wt% in Methanol) CAS number 68254-41-1, $C_{10}H_{14}F_3NO$ m-TFPTAH (commercially known as MethPrep II). Methylation has been widely used for the analysis of artists' media where it is useful for the analysis of both seed oils and natural resins which contain diterpenoid acids or triterpenoid acids such as moronic acid from mastic [29, 31–33]. MethPrep II methylation was achieved either: (1) by adding to the sample 1–3 drops of MethPrep II, depending on sample size, and heating at 60 °C for 24 h, or (2) by adding 30 µL of MethPrep II each 0.3 mg of sample and heating at 60 °C for 24 h. The MS Thermal programme (1), (2) or (3) were set for the analysis, as described hereafter. Thermal Programme (1). Seg1 start 2.40 Scan events MS, Heated zones Ion Source 250 °C, Detector Gain 1.21·105 (Multiplier Voltage 1025 V). Oven: Initial temp 40 °C hold 4 min Ramp 1 10.0 °C/min (rate), until 250 °C, hold 15 min. Mode: splitless. Thermal Programme (2). Seg1 start 2.40 Scan events MS, Heated zones Ion Source 250 °C, Detector Gain 1.21·105 (Multiplier Voltage 1025 V). Oven: Initial temp 40 °C hold 4 min Ramp 1 10.0 °C/min (rate), 250 °C, hold 45 min. The acquisition was carried out in a Total Ion Count mode, where all ions in the range 40–800 m/z were monitored. The Xcalibur™ 2.2 and PyroLab™ software were used to control the instruments. The former was then supported by the library browser supported NIST MS Version 2.0 [34] which facilitated data processing.

Dataset of analysis

A comprehensive dataset for the analysis of this object was deposited in Northumbria University's Figshare repository [23]. A full database of results in a spreadsheet format and with plots and figures was compiled. The description of the samples and images of the sampling site location can also be found in the dataset.

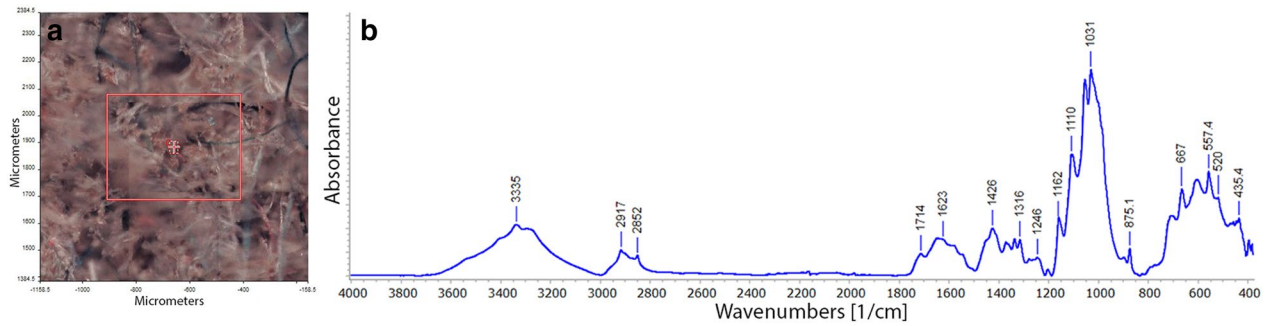

Fig. 5 Sample 1. Fibres of different colours are visible in the micrographs taken with Spotlight 400 FT-IR microscope (**a**). ATR-FT-IR analysis of the dust, baseline and Kubelka–Munk correction applied (**b**)

Results and discussion

The analyses were chosen to ensure the understanding of the coating materials, which was the scope of the research. However, a sample of incoherent dirt and dust was taken from the base of the tombstone (sample 1) and a sample of plaster bulk was taken from a deep crack (sample 2) to confirm the expected composition of the substrate. Samples 3 to 12 were taken so to be representative of the stratigraphy of the object from the surface to 0.5–1.0 mm towards the core of the object.

Dust

Dust deposited on the tombstone was sampled (Sample 1) and analysed to have a better understanding of the contaminants present in Gallery 46A, and eventually be able to discriminate which elements found on the surface can be attributed to the environmental dust in the galleries. Under the microscope, the sample seems to be mostly made of fibres of various colours (red, green, blue, Fig. 5). FT-IR analysis highlighted that the dust is made mostly of sulfates (such as gypsum and other varieties) with the asymmetric bending modes of SO_4 at 435, 600 and 667 cm^{-1}, the SO_4 symmetric and asymmetric stretching at about 1005 and 1105 cm^{-1} and the v_2 H_2O of the sulfates at about 1620 and 1680 cm^{-1} [35, 36]; carbonates (such as calcite) suggested by the peaks at 875 and 1425 cm^{-1} corresponding to out-of-plane bending and asymmetrical stretching vibration peaks of O–C–O [35, 37], respectively; silicates and other metal oxides generated several peaks in the fingerprint area [35, 38–41] and unidentified organic material(s) are suggested by the peaks in the 1200–1300 cm^{-1} area (v CN), the peaks at 1360 cm^{-1} (v CN aromatic amine), 1580 cm^{-1} (δ NH of amine I), 1714 cm^{-1} (v CO of esters) and the CH vibrational mode at 2852 and 2917 cm^{-1} [42, 43], possibly deriving from the fibres and other residues of human interaction (skin, oils and as such) [39, 42, 44] (Fig. 5). Overall, the sulfates and carbonates can be due to the building works, but the fibres and organic contribution derive from the visitor interactions.

Plaster bulk

The substrate (layer 0 in samples 3 to 13, as described in Table 1) largely consists of gypsum plaster (calcium sulfate, $CaSO_4 \cdot 0.5H_2O$), confirmed by EDS spectra and mapping (see for example sample 3 in Fig. 6). XRD analysis on all the samples also confirmed that the mineral gypsum is the main component in the sample, as shown for example in the diffractogram of sample 3 (Fig. 6) and indicated by the characteristic diffraction peaks in Table 2 and consistent with the gypsum references available in published databases [24, 25]. FT-IR spectra also showed the presence of gypsum plaster with the peaks at about 1005 and 1105 cm^{-1} (SO_4 symmetric and asymmetric stretching) and 1600 and 1680 cm^{-1} (v_2 H_2O of the sulfates), and also the sulfate overtones centred on 2220 cm^{-1} area, due to the combination of bending and vibration modes of H_2O ($v_1 + v_3$ and $2v_3$) related to the presence of gypsum [35, 36, 45, 46]. Aluminium (Al) was detected by EDS in all the layers of all the samples analysed and, as in the samples analysed as cross-sections, Al can be also due to the use of an Alumina suspension (Agar Scientific Micro-polish Alumina 0.3 µm—B8226) to obtain the final polish. Al is likely present, together with potassium (K) and silicon (Si) as part of silicate inclusions (visible in the EDS mapping and spectra, Fig. 7), which constitute clay minerals [47] and are reported to be present as a natural contaminant of mineral gypsum [2, 48]. FT-IR spectra suggest vibrations in the 950–1100 cm^{-1} region, characteristic of clay minerals (Si–O containing minerals, such as kaolin, $Al_2Si_2O_5(OH)_4$) [40, 47]. FT-IR peaks at 1440 and 1770 cm^{-1} (v CO_3) and overtone centred at 2400 cm^{-1} suggest the presence of calcite (calcium carbonate, $CaCO_3$), as suggested in other studies [26, 40, 43–45]. Minor variations of the position of the

Table 1 Summary of findings in the samples' layers

Sample	Type	Notes	No. of layers	Layers	Plaster	Interface	Coating	Overpaint
1	Dust	Fibres and mixture of organic and inorganic material	–	–	–	–	–	–
2	Plaster from the inner bulk		–	–	Calcium sulfate, calcium carbonate, clay minerals, Al, Mg, Si, diterpenic resin	–	–	–
3	Cross-section		3	2. Dark layer 1. Yellowish and undefined layer 0. Plaster bulk	Calcium sulfate, calcium carbonate, clay minerals, Mg, diterpenic resin	Intermediate of plaster and dark layer	Mostly Si and Al; Fe, Ti and traces of Na, Cl and K, diterpenic resin	–
4	Cross-section	Edge area of sampling	4	3. Purple layer 2. Dark layer 1. Yellowish and undefined layer 0. Plaster bulk	Calcium sulfate, calcium carbonate, clay minerals, Mg, diterpenic resin	Intermediate of plaster and dark layer	Mostly Si and Al, traces of K, Ba, Zn, Cl and P, diterpenic resin	Fe, Si and Ti, traces of K, Ba, Zn, Cl and P, drying oil modified alkyd paint
5	Cross-section		3	2. Dark layer 1. Yellowish and undefined layer 0. Plaster bulk	Calcium sulfate, calcium carbonate, clay minerals, Mg, Ti, diterpenic resin	Intermediate of plaster and dark layer	Mostly Si and Al, traces of Mg, Ti, Na, Fe and K, diterpenic resin	–
6	Cross-section	Area of repair	3	2. Dark layer 1. Yellowish and undefined layer 0. Plaster bulk	Calcium sulfate, calcium carbonate, clay minerals, Mg, Ti, traces of K and Fe, organic medium	Intermediate of plaster and dark layer	Mostly K, Fe, Si and Al, traces of Na, Pb and Cl, organic medium	–
7	Cross-section	Area of repair	2	1. Yellowish and undefined layer with large orange and black particles 0. Plaster bulk	Calcium sulfate, calcium carbonate, clay minerals, organic medium	–	Mostly Fe and Ba, traces of Mg, K and Cl, organic medium	–
8	Cross-section	Fluorescent varnish	4	3. Varnish 2. Dark layer 1. Yellowish and undefined layer 0. Plaster bulk	Calcium sulfate, calcium carbonate, clay minerals, Mg, Cl, diterpenic resin, possibly additional triterpenic resin or birch	Intermediate of plaster and dark layer	Mostly Si and Al, traces of K, Fe and Na, diterpenic resin, possibly additional triterpenic resin or birch	–

Table 1 (continued)

Sample	Type	Notes	No. of layers	Layers	Plaster	Interface	Coating	Overpaint
9	Cross-section		3	2. Dark layer 1. Yellowish and undefined layer 0. Plaster bulk	Calcium sulfate, calcium carbonate, clay minerals, Mg, Al, Sr and Fe, diterpenic resin, possibly additional triterpenic resin or birch	Intermediate of plaster and dark layer	Mostly Si, Al, Mg, Sr and Fe, traces of K and Ti, diterpenic resin, possibly additional triterpenic resin or birch	–
10	Cross-section		3	2. Dark layer 1. Yellowish and undefined layer 0. Plaster bulk	Calcium sulfate, calcium carbonate, clay minerals, Mg, organic medium	Intermediate of plaster and dark layer	Mostly Si and Al, traces of K and Cl, organic medium	–
11	Cross-section		4	3. Varnish 2. Dark layer 1. Yellowish and undefined layer 0. Plaster bulk	Calcium sulfate, calcium carbonate, clay minerals, Mg, organic medium	Intermediate of plaster and dark layer	Mostly Si and Al, traces of Fe and Mg, organic medium	–
12	Cross-section	Fluorescent varnish	4	3. Varnish 2. Dark layer 1. Yellowish and undefined layer 0. Plaster bulk	Calcium sulfate, calcium carbonate, clay minerals, Mg	Intermediate of plaster and dark layer	Mostly Si and Al, traces of P, Cl and Fe, organic medium	–
13	Cross-section	Fluorescent varnish	4	3. Varnish 2. Dark layer 1. Yellowish and undefined layer 0. Plaster bulk	Calcium sulfate, calcium carbonate, clay minerals, Mg, diterpenic resin	Intermediate of plaster and dark layer	Mostly Si and Al, traces of Fe, Mg, Cl, Ti and Na, diterpenic resin	–

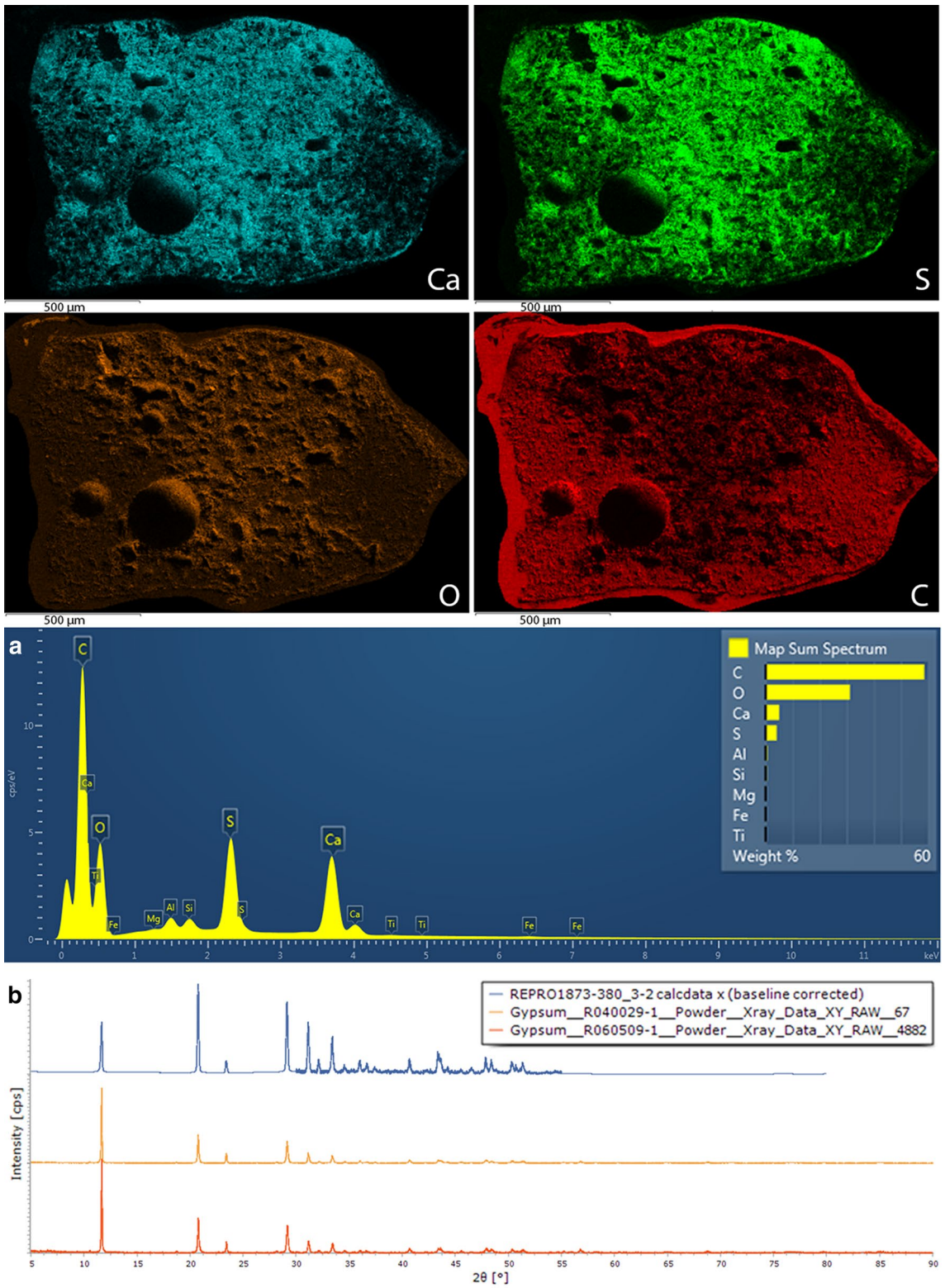

Fig. 6 EDS mapping and spectra (**a**) showed that sample 3 is made of calcium (Ca), sulfur (S) and oxygen (O) (calcium sulfate). Carbon (C) is present as detected from different sources (environment, casting polyester resin and organic media). XRD diffractogram (**b**) shows the characteristic peaks of gypsum, as also confirmed by comparison with the RUFF database [24] and COD Database [25]

Table 2 XRD peaks observed in the diffractograms of samples 2 and 3 and found in the RUFF database gypsum references R060509 and R040029

XRD peaks, 2θ [°]			
Sample 2	**Sample 3**	**R060509**	**R040029**
11.6304	11.67299	11.6688	11.6553
20.6882	20.74514	20.7682	20.7582
23.3816	23.37026	28.1588	28.1498
26.8718			
29.121	29.10739	29.1507	29.1396
31.0975	31.12382		
	32.09465		
33.4643	33.34622		
	34.53655		34.6194
	35.94149		35.9997
	36.65667	36.0027	36.65
	37.3434	37.4189	37.4124
40.5746	40.63457		
43.4695	43.38031		42.2079
	44.16252		44.2309
45.8294	45.51888	45.5453	45.5268
	46.495		46.4606
47.8711	47.85724	47.8955	47.8848
	48.35782	48.4221	48.3983
	48.72981		
	50.32856		
	50.73068		
	51.34237		
	54.41229		54.4676
	55.14868	55.2183	55.191
	55.81309		55.8618
56.6775	56.7291		
58.2058	58.19157		60.3599
	64.75298		
	65.8196		
67.0222	66.7291		66.7077
68.9538	68.66935		
	70.65909		
71.4685	71.22731		
	74.11747		
	76.56741		
	77.39589		
	79.61351		

FT-IR peaks related to the inorganic components can be observed for several reasons, one of which is the local substitution of elements such as Magnesium (Mg) and lead (Pb) in the gypsum and other minerals' structure [35, 40, 44, 45, 47]. Mg was also detected in all the samples by EDS and it is possibly an exchangeable element of the sulfate variety $MgSO_4$ (more or less hydrated, chalcanthite $CuSO_4{\cdot}5H_2O$, kieserite $MgSO_4{\cdot}H_2O$, starkeyite $MgSO_4{\cdot}4H_2O$, hexahydrite $MgSO_4{\cdot}6H_2O$, epsomite $MgSO_4{\cdot}7H_2O$ and meridianite $MgSO_4{\cdot}11H_2O$). Small quantities of sulfate varieties such as barite ($BaSO_4$), celestite ($SrSO_4$), anglesite ($PbSO_4$) and the Mg varieties mentioned above can be naturally present in the gypsum quarries or form after the rehydration of the gypsum plaster that occurs after the addition of water to the calcined powdered gypsum plaster [2, 47, 48]. These secondary mineral phases are commonly found in minerals [47] and, for example, suggested by trace studies on *stucco* objects [21]. This composition of the plaster was consistently found in layer 0 of samples 3–8 and 10–13 (Table 1). Sample 5 shows additional small inclusions of titanium (Ti) in the plaster bulk and sample 9 shows inclusions made of silicon (Si), aluminium (Al), iron (Fe) strontium (Sr) throughout the stratigraphy (Fig. 7). EDS mapping and XRD analysis confirmed that despite inclusions of calcium carbonate are present in the bulk, the object is largely made of gypsum plaster (made from gypsum) rather than lime plaster (made from calcite), which is instead often used for outdoor architectural details [4, 6], and was also found in the analysis of other casts [35]. Sample 2 was taken from the inner plaster bulk (about 5 cm from the surface), exposed on a deep crack of the tombstone, to understand whether the organic coating visible on the surface was also used as an additive in the plaster mixture, as suggested as possible by the historical literature [2, 48–50]. No organic materials were detected in sample 2 by FT-IR. Py-TMAH-GC/MS analysis indicated the presence of abietane skeleton diterpenoids due to the occurrence of the peaks at m/z 315, 299, 285, 253 and 239 (Fig. 8 and Table 3) [29, 51]: 7-Oxodehydroabietic acid, methyl ester at retention time, RT, 25.47 min and methyl dehydroabietate at 25.57 min in the chromatogram. The fragments at m/z 314 and 253 suggest the presence of a compound formed by oxidation of pine resin biomarkers, as suggested in several case studies [29, 51]. The peak at m/z 314 is related to the molecular ion of this degradation marker and the fragment at m/z 253 results from the loss of a methyl group followed by that of neutral formic acid [29]. The base peak at m/z 239 is reported as characteristic of the fragmentation of dehydroabietic acid [29]. This acid is the main degradation marker formed by the aromatisation of abietadienic acids, which are the major constituents of raw pine resins. Fatty Acids (FA) were also detected at 17.50 min (dimethyl azelate), 21.68 min (methyl palmitate) and 23.60 min (methyl stearate) (Table 3), as consistent with the relevant literature [27, 29]. The ratios azelate/palmitate (A/P = 0.7) and palmitate/stearate (P/S = 2.2) suggested that the resin has been mixed with an oil, or the FA are either from other

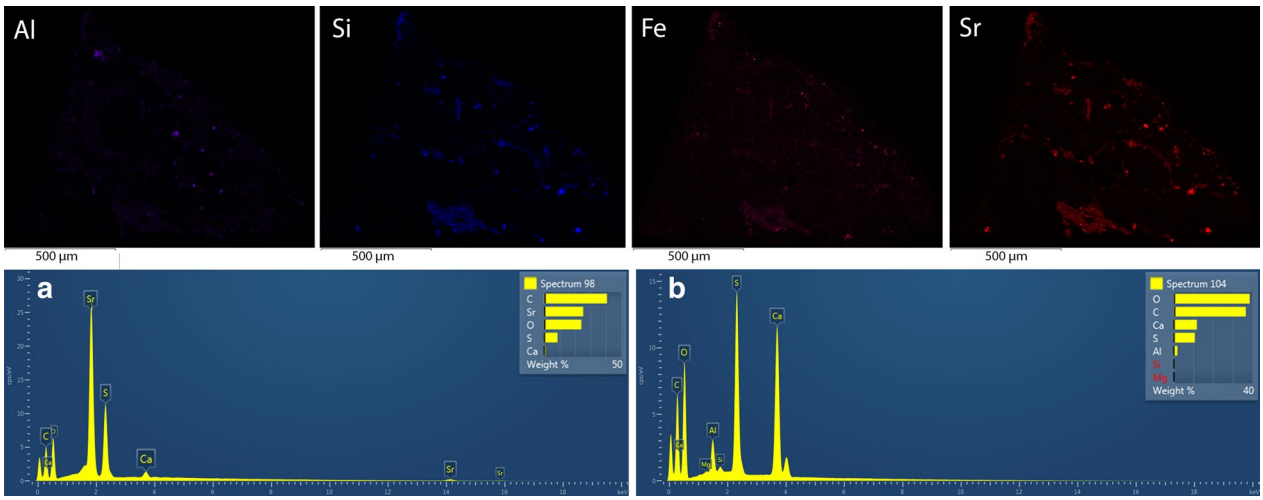

Fig. 7 Clay minerals (Al-Si silicates) are present in the stratigraphy of all the samples. EDS mapping and spectra (**a** and **b**) of sample 9 show the inclusions made of Aluminium (Al) and Silicon (Si), but also iron (Fe) and strontium (Sr). In other samples magnesium (Mg), titanium (Ti) and potassium (K) are present in the silicate inclusions

sources of lipids or naturally present in the resin [28, 29, 51]. It was suggested in other studies [52, 53] that the intensity of the FA peaks can change, as affected by matrix effects due to the presence of inorganic pigments. This would change the P/S ratio and therefore invalidate the correlation which allows the determination of the type of lipid. Due to the lack of previous studies on the effects of the predominance of the inorganic portion over the organic component on the areas of the FA peaks in the chromatogram, further research on this topic is required. Due to the complexity of the mixture, as often happen in the case of cultural heritage materials, separation methods are required prior the mass analysis so that several components arrive in the ion source one at a time [29]. For this reason, other peaks that can be assigned to small fragments of amine and lipids between 4.18 and 16.99 min in the chromatograms have not been considered diagnostic in this sample (Fig. 8). The full record of GC/MS results is provided in the dataset [23]. The inconsistency of the FT-IR and py-TMAH-GC/MS results in sample 2 may suggest that a very small quantity of resin was added in the plaster [2, 48] or that such small amount had penetrated deep in the plaster from the surface. It is also possible that the organic material derived from accidental contamination in the studio of the plasterer or it might have even been transferred from the mould during the casting process.

An interface layer, that appears yellow under visible light reflectance and possibly consists of a portion of the lower layer soaked with the surface coating(s), showing characteristics of both layers, is visible in samples 3–6 and 8–13 (Fig. 9). The tabular crystalline structure typical of gypsum plaster can be seen in the substrate layer and the interface layer in the BSE image [21, 47, 54]. In samples 10 and 11 the casting resin homogeneously penetrated the stratigraphy and in samples 3, 4, 5, 6, 8, 12 and 13 layer 1 appears 'denser' than layer 0 (Table 1), suggesting that the coating layer had penetrated the plaster, filling the pores and impeding the casting resin occupying the voids and possibly preserving the mineral structure of the gypsum plaster (Fig. 9). This was visible in the BSE image as well as through the EDS mapping (casting polyester resin and catalyst are mainly made of organic compounds C, H and O). The presence of the casting resin (polyester resin) was also detected in all the layers by FT-IR spectra (δ OH phenol at about 1312 cm^{-1} and δ CH aromatic at about 1760 cm^{-1}, as can be seen in the reference in Fig. 10).

Coating

Samples 3–5 and 8–13 show a coating layer, that appears dark under visible light reflectance (layer 2 in these samples as described in Table 1), and it likely consists of a pigmented organic medium and dirt. EDS mapping and spectra show that this dark layer contains calcium sulfate but consists mostly of Si and Al (Fig. 11). Traces of other elements can be seen and the composition varies from sample to sample (Table 1), suggesting that the trace elements in the surface layers derive from both the plaster substrate and the dirt deposited onto the surface. The presence of the polyester casting resin (Fig. 10) and gypsum plaster ($CaSO_4 \cdot 0.5\ H_2O$, characteristic peaks as described above) was detected in all the layers by FT-IR, including the surface. The presence of an

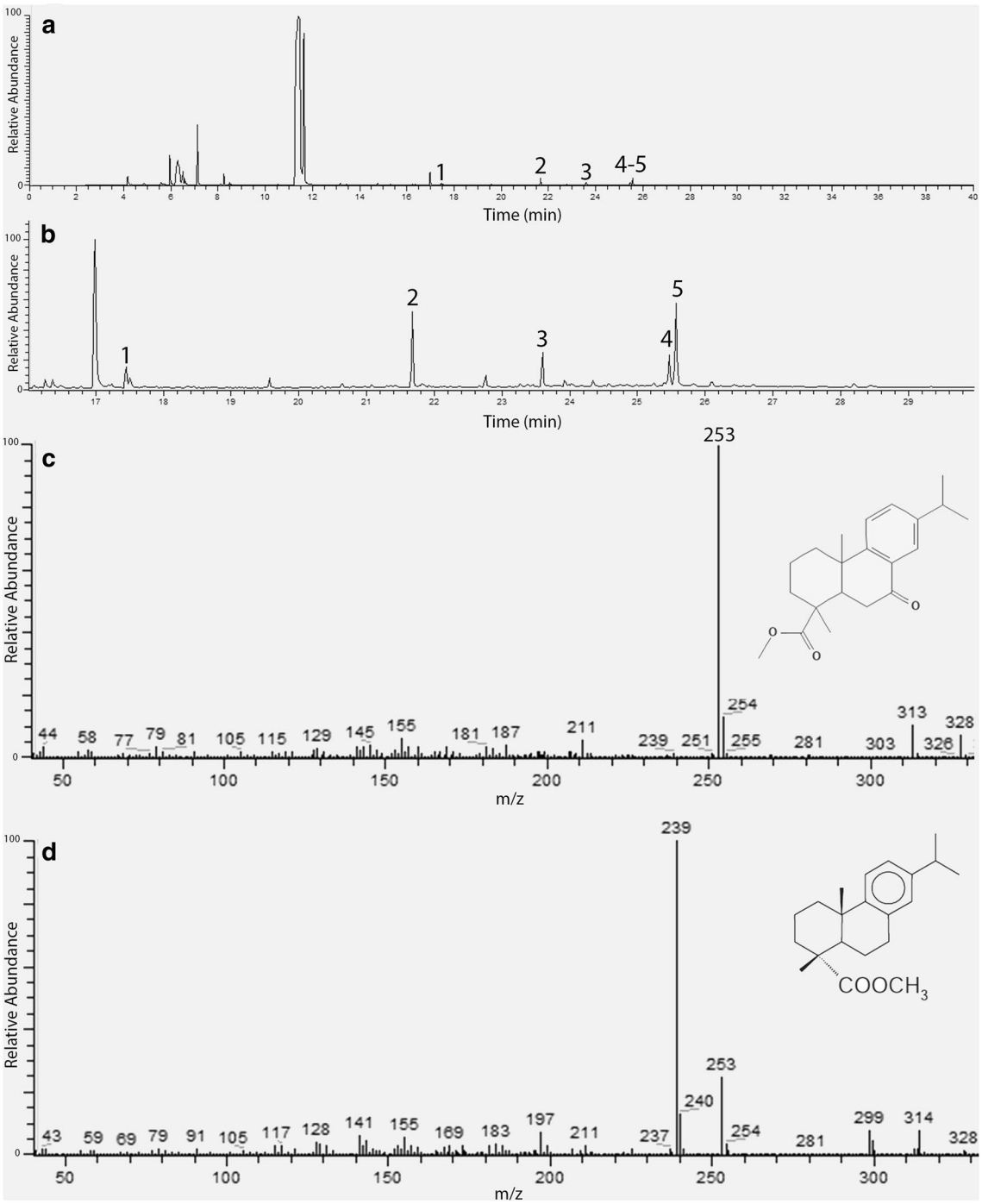

Fig. 8 py-TMAH-GC/MS chromatogram of sample 2 in the full retention time range, 0–40 min (**a**) and a narrower range, 16–30 min (**b**). The peaks up to 16.99 min are due to smaller lipid and amine fragments which are not diagnostic in this sample. The identification of pine resin was possible upon determination of the following markers: dimethyl azelate 1, methyl palmitate 2, methyl stearate 3, 7-oxo-dehydroabietic acid methyl ester 4 and methyl dehydroabietate 5. The mass spectra of compounds 4 (**c**) and 5 (**d**) are also shown

organic medium is indicated in all the FT-IR spectra and the position of the peaks suggest that is likely a wax or resin (CH bending and stretching); however, the crowded appearance of the spectra and the broadness of the peaks impede the unique assignment of such contributions. The several peaks that can be identified in the area over

Table 3 Most relevant py-TMAH-GC/MS mass spectrum fragmentation peaks for the materials characterization across the samples

RT (min)	m/z	Assignment
16.25	55, 69, 74, 83, 87, 111, 129(100), 138, 171, 188	Dimethyl phthalate
17.50	74(100), 87, 97, 111, 143, 152, 178, 185	Dimethyl azelate
21.68	74(100), 87, 101, 129, 145, 185, 227, 270	Methyl palmitate
23.60	74(100), 87, 129, 143, 199, 255, 298	Methyl stearate
25.47	187, 207, 253(100), 313, 328	7-Oxodehydroabietic acid, methyl ester
25.57	141, 155, 197, 239(100), 253, 314	Methyl dehydroabietate
30.08	79(100), 121, 138, 160, 189, 205, 442	Betullin

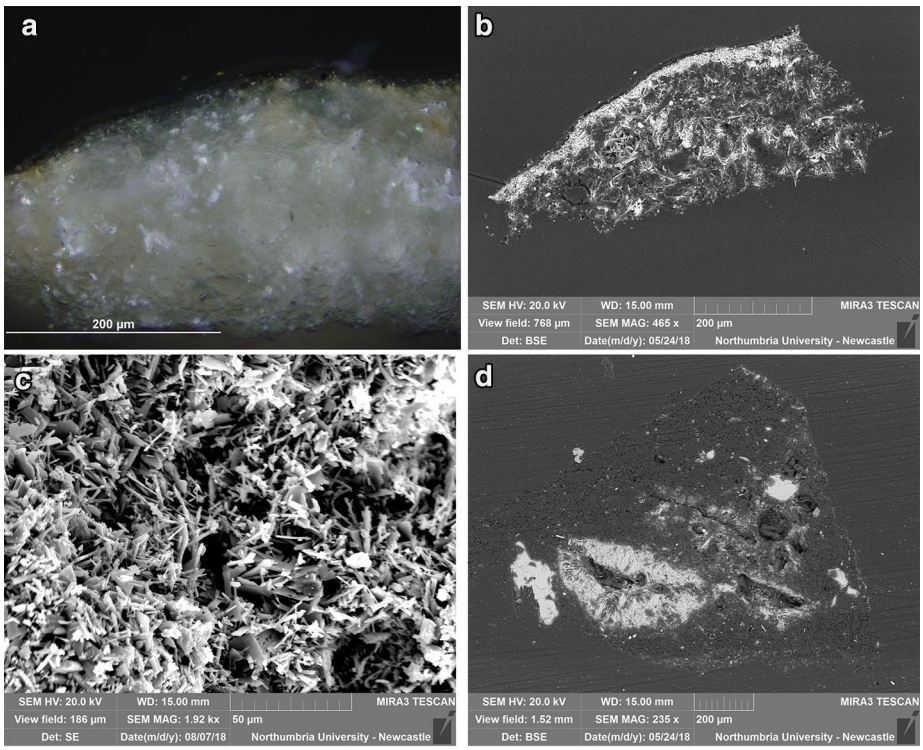

Fig. 9 High vacuum SEM–EDS (1.5×10^{-2} Pa) of sample 2 allowed a higher magnification; BSE image (**c**) shows the tabular structure of the gypsum plaster. SEM–EDS Low Vacuum Mode (10–15 Pa) of the samples cast in resin allowed to acquire the BSE image of the full stratigraphy. In sample 12 the *tabular* structure can be observed in layers 0 and 1 and layer 1 appears denser in the BSE image (**b**) and has a yellow tone under VLR OM (**a**). In sample 10 the BSE image (**d**) shows that the casting resin was absorbed evenly in the pores

3000 cm^{-1} cannot be considered uniquely diagnostic, as OH and NH stretches occur in this region and once again due to the complexity of the mixture, the water present in the crystals and the pores of the plaster, as well as in the organic components will add up in this area. Calcium oxalate might be also present in layer 2, but it was not possible to uniquely assign its peaks, as usually close to the vibrations characteristic of calcium sulfate, as also suggested in other studies [46]. Py-TMAH-GC/MS of samples 3, 4, 5, 8, 9 shows the markers characteristic of a diterpenic resin (similarly to sample 2, Fig. 8), such a rosin or pine resin, possibly mixed with a non-drying oil or another source of lipids, similar to what is suggested in relevant literature [27–29].

Py-TMAH-GC/MS of samples 8 and 9 shows peaks that were assigned, as based on previous studies [29, 55], to a betullin-like triterpene marker (at t = 30.08–33.49 min, Table 3), suggesting that, as rarely are diterpene and triterpene molecules are rarely found together in a plant resin, a birch, dammar or mastic is additionally

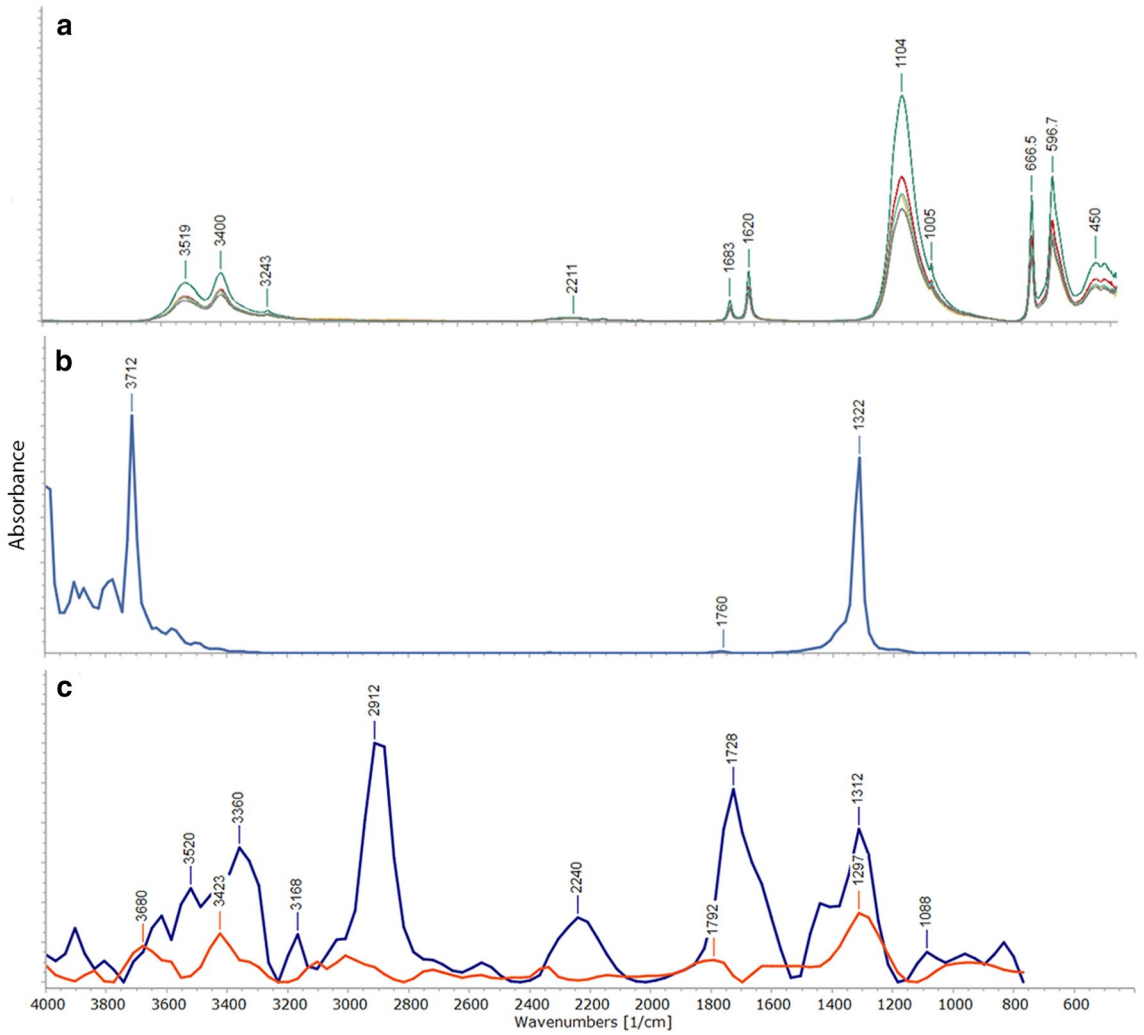

Fig. 10 FT-IR spectra acquired in ATR mode (gypsum plaster reference) (**a**), and in DR of polyester casting resin reference (**b**) and from layer 2 of sample 6 (orange line in **c**) and sample 9 (blue line in **c**)

present in the stratigraphy. The full fragmentation patterns of the markers characteristic of dammar and mastic were not detected, but this can be due to the natural degradation of the molecules or to the derivatization processes applied to the already degraded organic material, as suggested in [29, 56, 57] The small quantity of the organic material, when compared to the inorganic portion, also contributed to the small relative abundance of the di- and tri-terpene molecules in the chromatogram. The full record of GC/MS results is provided in the dataset [23].

The contributions of the organic material as shown in the FT-IR spectra of all the layers indicates that either the material was added to the wet gypsum plaster wet mixture or that the coating has also penetrated in the bulk. The latter seems also possible as the average depth of the samples is about 0.5 mm. The characterization of unknown organic materials in aged samples has been recognised as the most challenging application of GC/MS techniques [29]. Moreover, in sample 8 an additional layer (layer 3) fluoresces white under UV illumination, suggesting that these could be an additional layer or that layer 2 has not been absorbed evenly, as seen in the other samples. The same was also observed in samples 11, 12 and 13.

Areas of retouching

Sample 4 is characterised by the same stratigraphy described above but presents an additional layer (layer 3), purple under visible illumination (Fig. 12). EDS mapping suggested that this layer is mostly made of iron (Fe), silicon (Si) and titanium (Ti). Py-TMAH-GC/MS

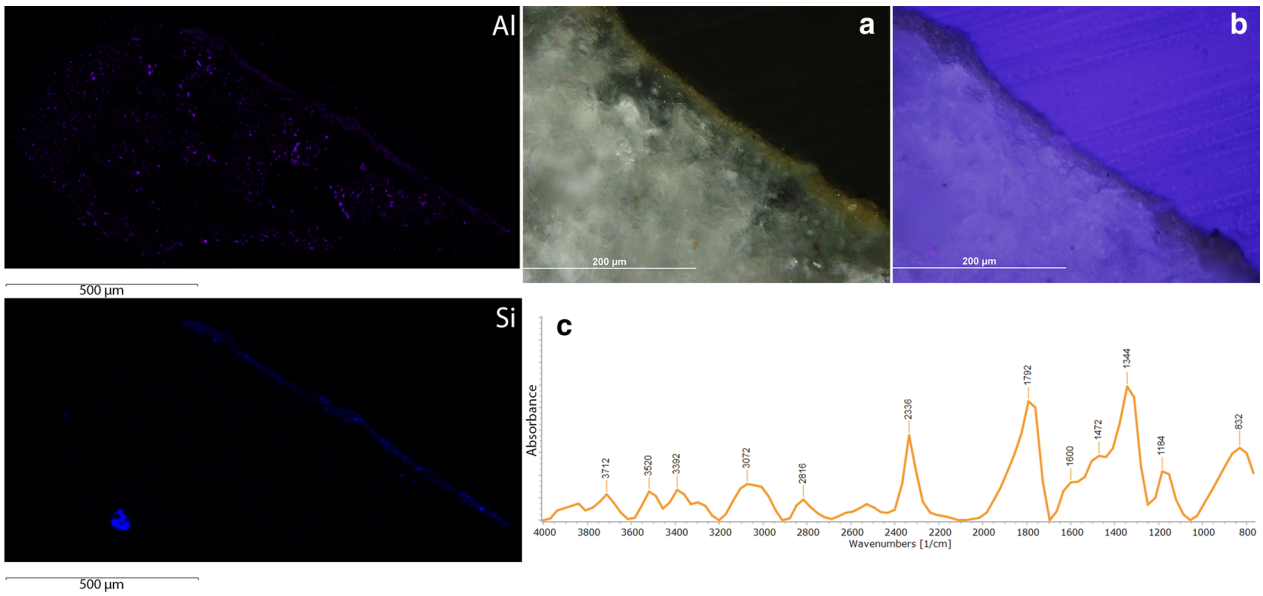

Fig. 11 Sample 11: the surface layer appears dark under VLR OM (**a**) and the interface layer is yellow under VLR OM. No characteristic fluorescence was observed in the UV-*f* OM (**b**). EDS mapping shows that the surface layer is mostly made of Si and Al. FT-IR analysis (**c**) shows a broad band that suggests the presence of gypsum, casting resin and an organic medium

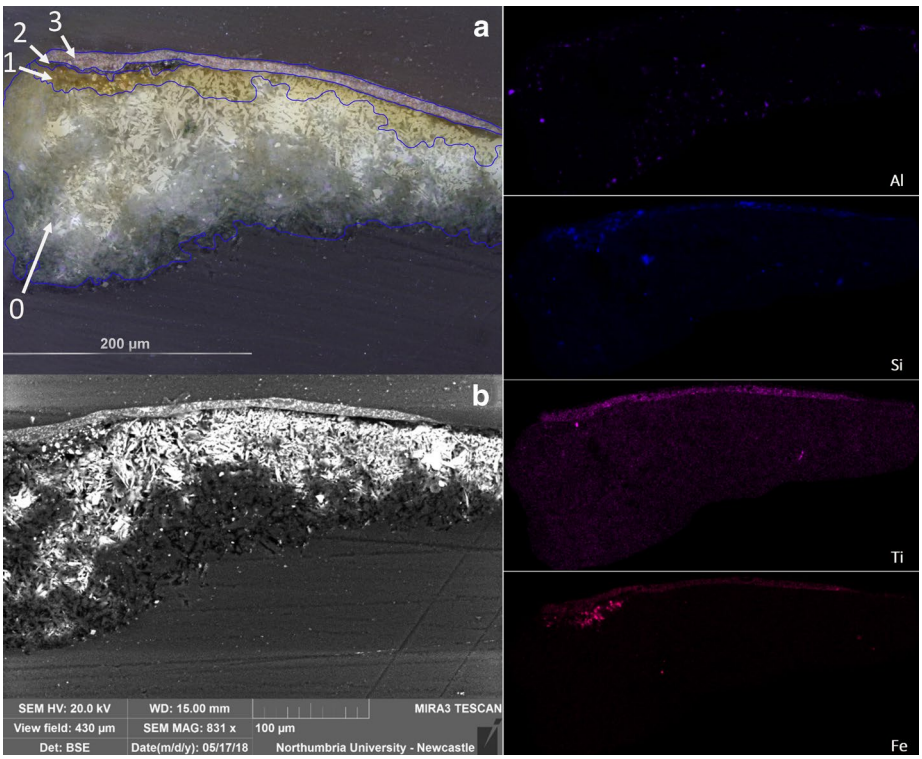

Fig. 12 Sample 4's VLR OM (**a**) and BSE images (**b**) and EDS mapping. The sample was taken from an area of overpaint. Al = aluminium, Si = silicon, Ti = titanium, Fe = iron

of this sample highlighted that a drying oil modified alkyd paint is the medium in this layer, suggesting that they were applied after the 1920s [30, 58, 59]. Dimethyl phthalate was detected at t = 16.25 min in the chromatogram (Table 3) and was considered a marker for aged alkyd paints mixtures, as it is reported to be forming in these paints upon ageing [30, 31]. Phthalic compounds can indicate the presence of a range of different twentieth-century materials. In art conservation they can be found, for example, in alkyd paints, polyvinyl adhesives and BEVA®371 and cellolyn [60]. Given that the phthalates were detected in the sample showing an additional refill and retouching layer and that V&A conservators have confirmed that polyvinyl adhesives, BEVA®371 and cellolyn are not documented as used in the Cast Courts,[2] it is postulated that the dimethyl phthalate is due to the presence of alkyd paints. Samples 6 and 7 broadly present the same stratigraphy of the other samples, however, the coating layer is made of K, Fe, Si and Al and traces of Na, Pb and Cl in sample 6 and Fe and Ba and traces of Mg, K and Cl in sample 7. In samples 8, 11, 12 and 13 an additional surface layer (layer 3 in these samples) fluoresces milky-white under UV illumination. No differences can be seen in the FT-IR spectra of these samples nor the GC/MS chromatograms, suggesting that either layer 3 is an additional layer of varnish made of the same material of the medium of layer 2 (diterpene resin) or layer 3 is an unabsorbed portion of the medium of layer 2 visible on the surface.

Manufacturing as suggested by the stratigraphy

In summary, the stratigraphy of the samples is quite consistent, featuring a 'substrate' layer, an 'interface' layer and a coating 'dark' layer, likely a combination of aged coating and dust. On top of these, some samples feature additional layers, having been overpainted or having been sampled from an area of repair. The bulk of the object is made of gypsum plaster, which contains several types of inclusions (including silicates and carbonates). By looking at the results, it is possible to hypothesise that in the surface layer, containing silicon and aluminium, but also traces of other elements, the medium is a diterpenic resin. Areas of repairs consist of overpaints made of alkyd paint, suggesting that they were applied after the 1920s [30, 58, 59], and inpaints containing silicon or barium. Areas showing an additional varnish layer might have locally highlighted or the additional layer might be due to a local difference in the surface absorbance or to an accidental spillage (as for example in sample 12, see Fig. 3).

[2] Personal communication with the V&A Conservation team (January 2021).

A summary of the results can be seen in Table 1 and has also been compiled in a comprehensive dataset [23].

Conclusions

A multi-analytical approach allowed the characterization of the surface coatings of the object. A 'substrate' layer made of gypsum plaster, an 'interface' layer and a coating 'dark' layer, likely a combination of aged diterpenic resin coating and dust were identified. Overpaint made of alkyd paint and areas of repair were also highlighted. Due to the immense variety of recipes for the manufacturing of the nineteenth-century plaster casts, the stratigraphy of a plaster cast might result in a complex combination of organic media and inorganic features, even more complex when modern treatments have been applied for the care of the cast. As a multi-analytical approach in studies on similar materials has been proven effective, the combination of techniques for the characterization of inorganic and organic components is fundamental in plaster artefacts. This study demonstrated that the suggested methodology for the characterisation of the coatings of historical plaster casts can provide information on nineteenth-century manufacturing. This case study suggests an analytical protocol that combines diverse methods to characterise the manufacturing of such artefacts. The investigation is ongoing and additional elements are still needed to have a comprehensive understanding of the cast manufacture and history, but the results discussed and summarised here demonstrate that despite the many analytical challenges of studying the complex composition of the cast, a thorough and comparative study can unveil the secrets of this nineteenth-century art. Further investigation is required to study the deterioration of those compounds on the sub-molecular level.

Abbreviations

BSE: Back Scattered Electron; EDS: Energy Dispersive Spectrometry; FT-IR: Fourier-Transform Infra-Red; FPA: Focal Plane Array; GCMS: Gas Chromatography–Mass Spectrometry; OM: Optical Microscopy; PL: Proper Left; PR: Proper Right; py: Pyrolysis; SEM: Scanning Electron Microscopy; TMAH: Tetramethylammonium hydroxide; UVF: Ultraviolet Fluorescence; VLR: Visible Light Reflectance; XRD: X-ay Diffraction.

Acknowledgements

Special thanks to the V&A: the Sculpture Conservation team for their insights on their conservation treatments and knowledge of the Cast Collection, and the Sculpture Curatorial Department for facilitating access to their collection and archival information.

Authors' contributions

Analyses were performed at the Northumbria University laboratories by VR under the supervision of CT. The project was initiated by CT and CH, who supervised the work in the Galleries. JP provided technical observations on the object. All authors read and approved the final manuscript.

Author details

Valentina Risdonne: Born in Italy, Heritage Scientist. B.Sc. (University of Perugia) and M.Sc. (University of Parma) in Sciences for the Conservation of Cultural

Heritage. AHRC CDP PhD student at Northumbria University and Victoria and Albert Museum. She occasionally has been collaborating with the V&A Science Section since 2015. Her research interests so far include lacquer object, pigments and plaster casts.

Charlotte Hubbard: Freelance sculpture conservator and consultant. Until 2019 she had been Head of Sculpture Conservation at the Victoria and Albert Museum for two decades. There she was latterly involved with the refurbishment of the Cast Courts and the creation of the new display of reproductions. She currently works on a range of traditional sculpture materials and acts as a consultant.

Johanna Puisto: Sculpture conservator at the Victoria & Albert Museum since 2005. She has worked on many of the Museum's projects conserving objects for several galleries including British Sculpture, Medieval and Renaissance, European Sculpture 1300–1600s, Buddhist Sculpture and The Cast Courts. She has also worked for the Museum's ceramics and metals conservation departments conserving objects for the ceramics and jewellery galleries and toys for the Museum of Childhood. Johanna graduated in 1996 with BA (Hons) in Conservation and Restoration from De Montfort University in Lincoln, where she specialised in the conservation of ceramics and ethnographic artefacts. Before joining the V&A she worked in the private sector conserving historic interiors including the St Paul's Cathedral and numerous other historic buildings, monuments and sculptures in the UK.

Charis Theodorakopoulos: PhD, is a conservation scientist and fine arts conservator. He is the Programme Leader of the MA Conservation and leads conservation science in the Department of Arts at Northumbria University, UK. His work focuses on the development and evaluation of conservation treatments for works of art and heritage objects, in particular, based on lasers and gel systems, the control of microclimates and the characterization of artists' materials.

Funding
This research was funded by the Art and Humanities Research Council (2017-21 AHRC/CDP Northumbria University and Victoria and Albert Museum—AH/R00322X/1) and supported by the Henry Moore Foundation (HMF Research and Travel Grant—2018).

Availability of data and materials
All data generated during this study are discussed in this published article and are fully available at the Figshare permanent data link: https://doi.org/10.25398/rd.northumbria.13469925.v3 [23].

Declarations

Competing interests
The authors declare that they have no competing interests.

Author details
[1]Department of Arts, Science in Conservation of Fine Art, Northumbria University, Burt Hall, Newcastle City Campus, NE1 8ST Newcastle upon Tyne, UK. [2]Conservation Department, Victoria and Albert Museum, Cromwell Rd., SW7 2RL London, UK. [3]Present Address: Independent conservator, London, UK.

Received: 16 February 2021 Accepted: 12 May 2021
Published online: 10 June 2021

References

1. Theodorakopoulos C, Hubbard C. VA-UNN CDP_2017_Casts. 2017. Internal Application Document.
2. Risdonne V, Hubbard C, Borges VHL, Theodorakopoulos C. Materials and techniques for the coating of nineteenth century plaster casts: a review of historical sources. Stud Conserv. 2021. https://doi.org/10.1080/00393630.2020.1864896.
3. Rotili V. La fortuna della copia in gesso: teoria e prassi tra Sette e Ottocento, PhD Thesis. Università degli studi Roma Tre. 2009.
4. Lending M. Plaster monuments: architecture and the power of reproduction. New Jersey: Princeton University Press; 2017.
5. Frederiksen R, Marchand E. Plaster casts: making, collecting and displaying from classical antiquity to the present, vol. 18. Berlin: Walter de Gruyter; 2010.
6. Bankart GP. The Art of the plasterer. An account of the decorative development of the craft, chiefly in England from the XVIth to the XVIIIth century, with chapters on the stucco of the classic period and of the Italian Renaissance, Also on scraffito, pargeting, Scot . London: BT Batsford; 1908.
7. Millar W. Plastering, plain & decorative. A practical treatise on the art & craft of plastering and modelling, including full description of the various tools, materials, processes and appliances employed. London: Donhead Publishing Ltd; 1899. (**Reprint**).
8. Guderzo M, Lochman T. Il valore del gesso come modello, calco, copia per la realizzazione della scultura, 2–3 ottobre 2015. Possagno: Antiga Edizioni; 2017.
9. Wade R. The production and display of Domenico Brucciani's plaster cast of Hubert Le Sueur's equestrian statue of Charles I. Sculpt J. 2014;23(2):250.
10. Werner N, Schmitz W. Giessener Beiträge zur Kunstgeschichte. Giessen: Schmitz; 1973.
11. Valmen H. General lexicon of visual artists from antiquity to the present, vol. 22. Leipzig: Krugner-Leitch-Sailor; 1928.
12. V&A website—Search the collections. 2020. https://collections.vam.ac.uk/. Accessed 20 Dec 2020.
13. Haskell F, Penny N. Taste and the antique: the lure of classical sculpture, 1500–1900. London: Yale University Press; 1981.
14. Marcinkowski W, Zaucha T. Kraków na wyciągnięcie ręki. Rzeźba architektoniczna ze zbiorów Muzeum Narodowego w Krakowie/Krakow within your reach. Architectural sculpture in the collection of the National Museum in Krakow. Krakow: MNK; 2010.
15. Payne EM. The conservation of plaster casts in the nineteenth century. Stud Conserv. 2020;65(1):37–58.
16. Pelosi C, Fodaro D, Sforzini L, Rubino AR, Falqui A. Study of the laser cleaning on plaster sculptures. The effect of laser irradiation on the surfaces. Opt Spectrosc. 2013;114(6):917–28.
17. Freire MT, Santos Silva A, Veiga MD, Dias CB, Manhita A. Stucco marble in the Portuguese architecture: multi-analytical characterisation. Int J Archit Herit. 2020. https://doi.org/10.1080/15583058.2020.1765051.
18. Salavessa E, Jalali S, Sousa LMO, Fernandes L, Duarte AM. Historical plasterwork techniques inspire new formulations. Constr Build Mater. 2013;48:858–67.
19. Luxán MP, Dorrego F, Laborde A. Ancient gypsum mortars from St. Engracia (Zaragoza, Spain): characterization. Identification of additives and treatments. Cem Concr Res. 1995;25(8):1755–65.
20. Megens L, Joosten I, Tagle AD, Dooijes R. The composition of plaster casts. 2011. http://www.kennisvoorcollecties.nl/en/projects/objects-in-context/conservation-of-plaster-collections/. Accessed 20 Dec 2020.
21. Gariani G, et al. First insights on the mineral composition of 'stucco' devotional reliefs from Italian Renaissance Masters: investigating technological practices and raw material sourcing. J Cult Herit. 2018;34:23–32.
22. Klosowska A, Obarzanowski M. Plaster casts in the collection of the National Museum in Krakow. Conservation issue. In: Plaster casts of the works of art. History of collection, conservation, exhibition practice. Krakow: National Museum Krakow, Muzeum Naradowe w Krakowie; 2010.
23. Risdonne V, Theodorakopoulos C. Database of Results. V&A cast of the tombstone of the Presbyter Bruno (REPRO.1873-380). Northumbria University, Newcastle upon Tyne. 2021. https://doi.org/10.25398/rd.northumbria.13469925.v3.
24. Lafuente B, Downs R, Yang H, Stone N. The power of databases: the RRUFF project. In: Armbruster T, Danisi RM, editors. Highlights in mineralogical crystallography. Berlin: Walter de Gruyter; 2015. p. 1–29.
25. Gražulis S, et al. Crystallography open database—an open-access collection of crystal structures. J Appl Crystallogr. 2009;42(4):726–9.
26. Sotiropoulou S, et al. Advanced analytical investigation on degradation markers in wall paintings. Microchem J. 2018;139:278–94. https://doi.org/10.1016/j.microc.2018.03.007.
27. Ribechini E, Modugno F, Colombini MP, Evershed RP. Gas chromatographic and mass spectrometric investigations of organic residues from Roman glass unguentaria. J Chromatogr A. 2008;1183(1–2):158–69.

28. Mills JS. The gas chromatographic examination of paint media. Part 1. Fatty acid composition and identification of dried oil films. Stud Conserv. 1966;11(2):92–107. https://doi.org/10.2307/1505447.
29. Colombini MP, Modugno F. Organic mass spectrometry in art and archaeology. Hooboken: Wiley; 2009.
30. Wei S, Pintus V, Schreiner M. A comparison study of alkyd resin used in art works by Py-GC/MS and GC/MS: the influence of aging. J Anal Appl Pyrol. 2013;104:441–7.
31. Singer B, McGuigan R. The simultaneous analysis of proteins, lipids, and diterpenoid resins found in cultural objects. Annali di Chimica. 2007;97(7):405–17.
32. Challinor JM. The development and applications of thermally assisted hydrolysis and methylation reactions. J Anal Appl Pyrol. 2001;61(1–2):3–34.
33. Challinor JM. The scope of pyrolysis methylation reactions. J Anal Appl Pyrol. 1991;20:15–24.
34. Linstrom PJ, Mallard WG. NIST chemistry WebBook, NIST standard reference database number 69, National Institute of Standards and Technology, Gaithersburg, MD, 20899. 2014.
35. Melita L, Węgłowska K, Tamburini D. Investigating the potential of the Er: YAG laser for the removal of cemented dust from limestone and painted plaster. Coatings. 2020;10:1099. https://doi.org/10.3390/coatings10111099.
36. Miliani C, Rosi F, Daveri A, Brunetti BG. Reflection infrared spectroscopy for the non-invasive in situ study of artists' pigments. Appl Phys A. 2012;106(2):295–307.
37. Hajji S, Turki T, Boubakri A, Ben Amor M, Mzoughi N. Desalination and Water Treatment Study Of Cadmium adsorption onto calcite using full factorial experiment design. Desalination Water Treat. 2017;83:222–33. https://doi.org/10.5004/dwt.2017.21079.
38. Aïssa B, Isaifan RJ, Madhavan VE, Abdallah AA. Structural and physical properties of the dust particles in Qatar and their influence on the PV panel performance. Sci Rep. 2016;6:31467.
39. Kumar RS, Rajkumar P. Characterization of minerals in air dust particles in the state of Tamilnadu, India through FTIR, XRD and SEM analyses. Infrared Phys Technol. 2014;67:30–41.
40. Beran A. Infrared spectroscopy of micas. Rev Mineral Geochem. 2002;46(1):351–69.
41. Hofmeister AM, Bowey JE. Quantitative infrared spectra of hydrosilicates and related minerals. Mon Not R Astron Soc. 2006;367(2):577–91.
42. Derrick MR, Stulik D, Landry JM. Infrared spectroscopy in conservation science. Malibu: Getty Publications; 2000.
43. Vahur S, Teearu A, Peets P, Joosu L, Leito I. ATR-FT-IR spectral collection of conservation materials in the extended region of 4000–80 cm^{-1}. Anal Bioanal Chem. 2016;408(13):3373–9.
44. Price BA, Pretzel B, Lomax SQ. Infrared and raman users group spectral database. 2007th ed. Philadelphia: IRUG; 2009.
45. Manfredi M, Barberis E, Rava A, Robotti E, Gosetti F, Marengo E. Portable diffuse reflectance infrared Fourier transform (DRIFT) technique for the non-invasive identification of canvas ground: IR spectra reference collection. Anal Methods. 2015;7(6):2313–22.
46. Toniolo L, Zerbi CM, Bugini R. Black layers on historical architecture. Environ Sci Pollut Res. 2009;16(2):218–26. https://doi.org/10.1007/s11356-008-0046-8.
47. Cox KG, Price NB, Harte B. An introduction to the practical study of crystals, minerals, and rocks. London: Halsted Press; 1974.
48. Turco A. Il Gesso. Lavorazione, trasformazione, impieghi. Milan: Hoepli; 1990.
49. Auerbach A. Modelled sculpture and plaster casting. New York: Thomas Yoseloff; 1961.
50. Meilach DZ. Creating with plaster. London: Blandford Press; 1966.
51. Mills J, White R. Organic chemistry of museum objects. London: Routledge; 2012.
52. Chiavari G, Fabbri D, Prati S. Effect of pigments on the analysis of fatty acids in siccative oils by pyrolysis methylation and silylation. J Anal Appl Pyrol. 2005;74(1):39–44. https://doi.org/10.1016/j.jaap.2004.11.013.
53. Poli T, Piccirillo A, Zoccali A, Conti C, Nervo M, Chiantore O. The role of zinc white pigment on the degradation of shellac resin in artworks. Polym Degrad Stab. 2014;102:138–44.
54. Aquilano D, Otálora F, Pastero L, García-Ruiz JM. Three study cases of growth morphology in minerals: halite, calcite and gypsum. Prog Cryst Growth Charact Mater. 2016;62(2):227–51.
55. Van der Doelen GA. Molecular studies of fresh and aged triterpenoid varnishes. University of Amsterdam. PhD Thesis. 1999.
56. Colombini MP, Bonaduce I, Gautier G. Molecular pattern recognition of fresh and aged shellac. Chromatographia. 2003;58(5):357–64. https://doi.org/10.1365/s10337-003-0037-3.
57. Coelho C, Nanabala R, Ménager M, Commereuc S, Verney V. Molecular changes during natural biopolymer ageing—the case of shellac. Polym Degrad Stab. 2012;97(6):936–40.
58. Duce C, Bernazzani L, Bramanti E, Spepi A, Colombini MP, Tiné MR. Alkyd artists' paints: do pigments affect the stability of the resin? A TG and DSC study on fast-drying oil colours. Polym Degrad Stab. 2014;105:48–58.
59. İşeri-Çağlar D, Baştürk E, Oktay B, Kahraman MV. Preparation and evaluation of linseed oil based alkyd paints. Prog Org Coat. 2014;77(1):81–6.
60. Horie CV. Materials for conservation: organic consolidants, adhesives and coatings. London: Routledge; 2010.

Publisher's Note